Thickness independent vibrational thermal conductance across confined solid-solution thin films

Ashutosh Giri,[*,†] Ramez Cheaito,[‡] John T. Gaskins,[‡] Takanori Mimura,[¶]
Harlan J. Brown-Shaklee,[§] Douglas L. Medlin,[∥] Jon F. Ihlefeld,[§] and
Patrick E. Hopkins[*,‡]

†*Department of Mechanical, Industrial and Systems Engineering, University of Rhode Island,
Kingston, RI 02881, USA*

‡*Department of Mechanical and Aerospace Engineering, University of Virginia, Charlottesville,
VA 22904, USA*

¶*Department of Materials Science and Engineering, University of Virginia, Charlottesville, VA
22904, USA*

§*Sandia National Laboratories, Albuquerque, NM 87123, USA*

∥*Sandia National Laboratories, Livermore, VA 94550, USA*

⊥*Charles L. Brown Department of Electrical and Computer Engineering, University of Virginia,
Charlottesville, VA 22904, USA*

#*Department of Physics, University of Virginia, Charlottesville, VA 22904, USA*

E-mail: ashgiri@uri.edu; phopkins@virginia.edu

Abstract

We experimentally show that the thermal conductance across confined solid-solution crys-
talline thin films between parent materials does not necessarily lead to an increase in thermal

resistances across the thin film geometries with increasing film thicknesses, which is counterintuitive to the notion that adding material serves to increase the total thermal resistance. Confined thin epitaxial $Ca_{0.5}Sr_{0.5}TiO_3$ solid-solution films with systematically varying thicknesses in between two parent perovskite materials of calcium titanate and (001)-oriented strontium titanate are grown and thermoreflectance techniques are used to accurately measure the thermal boundary conductance across the confined solid-solution films showing that the thermal resistance does not substantially increase with the addition of solid-solution films with increasing thicknesses from ~1 nm to ~10 nm. Contrary to the macroscopic understanding of thermal transport where adding more material along the heat propagation direction leads to larger thermal resistances, our results potentially offer experimental support to the computationally predicted concept of vibrational matching across interfaces. This concept is based on the fact that a better match in the available heat carrying vibrations due to an interfacial layer can lead to lower thermal boundary resistances, thus leading to an enhancement in thermal boundary conductance across interfaces driven by the addition of a thin "vibrational bridge" layer between two solids.

Keywords: Thermal boundary conductance, Interfacial solid-solution films, vibrational bridge, thermal conductivity, perovskite oxides.

Introduction

Disorder and imperfections, in general, lead to a decrease in thermal transport by inducing phonon scattering that limits the mean free path. In homogeneous materials, this has been studied for more than a century dating back to Einstein's original treatment of thermal conductivity of solids being driven by "atomic spacing" limited vibrations of uncorrelated oscillators.[1] This concept has since manifested itself in theories for thermal conductivity of disordered and amorphous solids, often deemed the "minimum limit" to thermal conductivity.[2,3] This is fitting for most materials, as disorder that causes vibrational dephasing and resistance on the order of one atomic spacing will result in a drastic reduction in thermal conductivity compared to crystalline counterparts. However,

this concept is complicated at solid interfaces, since thermal transport across solid-solid interfaces, quantified by the thermal boundary conductance (h_{K}),[4,5] is considerably driven by the intrinsic vibrational and phononic properties of the two materials comprising each side of the interface.[6] Therefore, introduction of disorder in the vicinity of material interfaces adds additional complexity to an already complicated problem.

Several prior works have demonstrated the wide variability of h_{K} with material and interfacial properties such as mismatch of phonon spectra,[7–11] interfacial chemistry and bonding,[12–20] crystallographic orientation,[10,21–23] interfacial structure,[12,16,24–30] and impurity regions.[16,31–34] In most cases, interfacial "imperfections" have been observed to lead to a decrease in thermal boundary conductance.[6,20,35] For example, we have observed this decrease in thermal boundary conductance across interfaces with roughness (i.e., geometric disorder),[12] an amorphous layer (i.e., structural disorder),[36,37] and elemental mixing resulting in both compositional and structural disorder.[38] In each of these cases, the specific disorder led to a reduction in thermal boundary conductance. Moreover, crystallographic interfaces introduced through tilt grain boundaries and nanostructuring have also shown to reduce the effective thermal conductivity.[39,40]

However, recent computational and experimental works have shown that with specific tailoring of this interfacial disorder, an increase in thermal boundary conductance across solid interfaces can be realized.[16,29–32,34,41–47] For example, atomistic simulations have shown that a thin crystalline interfacial region between two solids can bridge the vibrational states and lead to an increase in phonon transmission and thermal boundary conductance.[34,41,42] In our previous works, we observed both computationally[32] and experimentally[43] an increase in thermal boundary conductance by introducing mass impurities at a crystalline interface. In essence, this disordered region created a "mass-bridge" that led to a grading of oscillations across the solid interface, leading to a structurally disordered interface having a higher thermal boundary conductance than a more "perfect" interface. Recently, there have been several works that have taken this finding to the limit of complete disorder by demonstrating both computationally[29,30,44,45,48] and experimentally[16,46,47] that the thermal boundary conductance across a disordered interface can be much higher than

those for interfaces composed of crystalline materials. In this limit, lack of periodicity in the amorphous phase leads to a relatively featureless vibrational density of states, which increases the overlap in the density of states of heat carrying vibrations between the two materials comprising the interface in comparison to the case of two crystalline materials. Furthermore, the existence of interfacial modes localized near the interface between two solids (which are not present in the bulk of the materials) has also been shown to be an additional channel to enhance interfacial heat transport. [16,22,49–51]

The results in these aforementioned works demonstrate the unique atomic conditions and structures that can lead to increases in thermal boundary conductance, but most rely on conditions of atomic disorder or roughness. Still, the experimental realization of the originally posed computational concept of the so-called "phonon bridge", or the ability to insert a third material in between two materials at an interface to increase h_{K}, has been limited to metallic adhesion layers [17,18,26,27,36,52] and across self-assembled monolayers with different length of alkane chains (that are either sandwiched between thin metallic layers or between a metal layer and a semiconductor substrate). [53–55] For the later, it has been shown that the length of the self-assembled monolayers does not dictate heat transfer and rather the bonding at the end-group drives the increase in conductance across the interfaces. [15,53–55] Yet, heat transfer across confined thin films in between two semiconducting or insulating materials has never been studied experimentally, which is the aim of the current work. Here, we experimentally demonstrate that the thermal conductance across confined solid-solution thin films between parent semiconducting materials does not necessarily lead to a change in the overall thermal conductance between the parent materials, which is counterintuitive to the notion that adding material usually results in a decrease in thermal conductance. We posit that by considering an interfacial solid-solution film between two materials, the "phonon-bridge" concept can potentially be realized in insulating crystalline materials, which would establish a new phase space for realization of this concept in a wide array of material systems. However, we note that for the material systems studied in this work, the conductance is found to be independent of the thickness of the confined solid-solution thin film.

Much like the thermal boundary conductance across crystalline/amorphous interfaces, the spectrally broadened features in the density of states of an alloy would lead to an increase in thermal boundary conductance across each alloy film interface as compared to a single crystalline/crystalline interface. Furthermore, the long wavelength-dominated thermal conductivity in alloys leads to relatively large thickness regimes of thin films in which ballistic phonon transport dominates the thermal conductivity.[56] This translates to the thermal resistance of the alloy film (approximated by d/κ, where d is the alloy film thickness and κ is its thermal conductivity), which remains constant as thickness is increased. This is in stark contrast to thickness trends in thermal resistance in the diffusive limit of materials, where the resistance increases linearly with the thickness of the material as the intrinsic thermal conductivity of the material remains unchanged. To test the aforementioned hypothesis, we measure the thermal boundary conductance across single crystalline $CaTiO_3$ (CTO)/$SrTiO_3$ (STO) interfaces with varying thicknesses of single crystalline $Ca_{0.5}Sr_{0.5}TiO_3$ (CSTO) interfacial confined thin solid-solution films with disorder on the perovskite A-site (i.e. the Ca/Sr lattice site). Another motivation to study heat transfer across these material systems rests on the fact that heterostructures of perovskite oxides are emerging in a wide range of electronic applications[57] such as in interfacial superconductivity,[58] ferromagnetism,[59] and for high mobility electron gas at the heterointerface.[60] Furthermore, STO has been widely used as substrate for growing functional oxides.[61,62] Therefore, it is quintessential for these applications to understand thermal transport across interfaces comprised of such perovskite oxides. In this study, we find that the thicker solid-solutions do not lead to higher overall resistances across the solid-solution interfacial films and, in fact, the thermal boundary conductances across the CTO/CSTO/STO interfaces are relatively constant regardless of the CSTO thickness. We discuss the different factors that could influence our experimentally observed constant h_K (within uncertainties) across the various thicknesses of CSTO films.

Sample fabrication and structural characterization

Epitaxial CTO and CSTO films were prepared on TiO_2-terminated (001)-oriented STO single crystal substrates[63] (CrysTec GmbH) via 30° off-axis rf magnetron sputtering in a custom growth system. A substrate temperature of 700 °C and background pressure comprising 20 mTorr of 5:1 $Ar:O_2$ was used for all depositions. A 25 mm diameter CSTO target was prepared via conventional solid-state synthesis procedures. CSTO layers were deposited with a 30 W sputter power. A commercially-purchased 75 mm diameter CTO target was used for the CTO growth with a sputter power of 225 W. The thicknesses of the CSTO layers varied from 1 to 10 nm and the CTO layer on all films was 130 nm thick and growth rates were 0.3 and 0.46 nm/min, respectively. The CTO layers were all grown in the same deposition run to ensure that the CTO was identical in each case. Nominally 90 nm thick platinum films were deposited via rf magnetron sputtering to serve as transducers for the thermoreflectance measurements and were also prepared in the same deposition run.

Out-of-plane film orientation was measured with X-ray diffraction (XRD) using a Philips X'Pert MPD instrument with Cu Kα radiation as shown in Fig. 1a. Only the peaks attributed to the CTO film and STO substrate could be observed and the CSTO films could not be differentiated as these layers are relatively much thinner and the lattice spacings are not sufficiently different such that its reflections would overlap the film and substrate reflections. XRD pole figures were collected for the 202 reflections of both the STO substrates and CTO films for each sample using a Rigaku SmartLab instrument with Cu Kα radiation in a parallel beam configuration. The results for the CTO films with 10 nm and 1 nm thickness CSTO layers and the STO substrate are shown in Fig. 1b, 1c, and 1d, respectively. Also shown in Fig. 1e is a 2θ-ω pattern for the 202 reflections of the substrate and CTO film for the 5 nm CSTO sample. Separation of the 202 peaks is observed in the 2θ-ω scan and the pole figures provide clear evidence that the 4-fold symmetry of the substrate and film is observed in each case, which demonstrates epitaxial growth. Film surface topography of the STO substrate and CSTO films was characterized by contact mode atomic force microscopy using a Park Scientific Autoprobe CP instrument. The surface topography of the 10
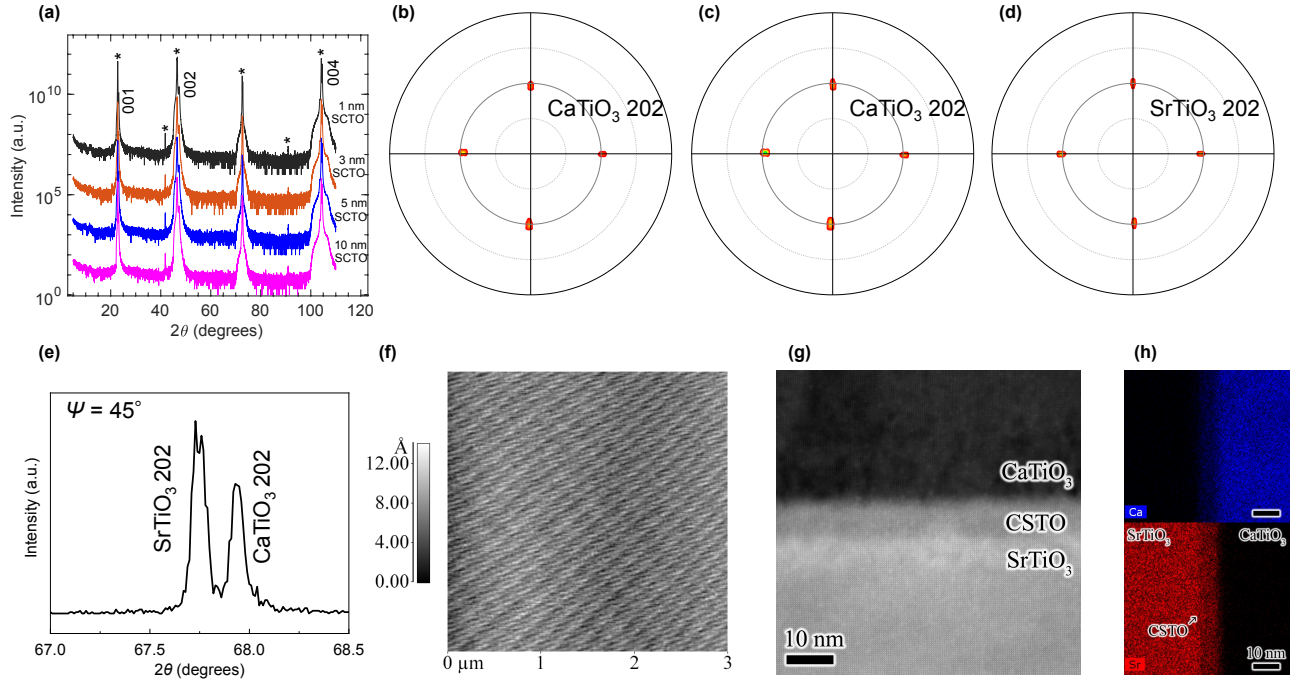
Figure 1: (a) The θ-2θ XRD patterns for the films, which shows that only peaks attributed to the SrTiO$_3$ substrate and CaTiO$_3$ film could be observed. The peaks indicated by '*' denotes substrate reflections. XRD pole figures for (b) 10 nm, (c) 1 nm CSTO and (d) STO substrate. (e) 2theta-omega pattern for the 202 reflections of the substrate and CTO film for the 5 nm CSTO sample. (f) The surface topography of the 10 nm CSTO film after deposition and before CaTiO$_3$ growth showing clear atomic steps, which indicates that pseudomorphic growth was achieved. (g) High resolution TEM image and (h) STEM-EDS maps of the 10 nm CSTO sample confirms film CSTO layer thickness and abruptness of the interfaces. Clear abrupt interfaces are observed in both the high-resolution image and the EDS maps for all films, showing the transition from pure SrTiO$_3$ to Ca$_{0.5}$Sr$_{0.5}$TiO$_3$ to CaTiO$_3$ with lattice registry across both interfaces.

nm CSTO film after deposition and before CTO growth is shown in Fig. 1f, which shows clear atomic steps indicating that pseudomorphic growth was achieved. Prior to CTO deposition, atomic force microscopy was used to obtain surface RMS roughnesses, which are approximately 2 Å for all CSTO films (see Supporting Information for details) and is the same as the STO substrate prior to CSTO deposition.

CSTO film thickness and epitaxy was confirmed via scanning transmission electron microscopy (STEM) and energy dispersive spectroscopy (STEM-EDS) with a FEI Titan^{TM} G2 80-200 STEM equipped with a Cs probe corrector, high-angle annular dark-field detector, a ChemiSTEM^{TM} technology X-FEG^{TM} and SuperX^{TM} EDS with four windowless silicon drift detectors. The high resolution TEM and STEM-EDS maps for the 10 nm CSTO showing clear transition from pure STO to CSTO to CTO with lattice registry across both interfaces is shown in Figs. 1g and 1h, respectively. Cross section samples were prepared via focused ion beam milling.

Thermal characterization

We perform simultaneous measurements of time domain thermoreflectance (TDTR) and frequency domain thermoreflectance (FDTR) to measure the overall thermal conductance across the solid-solution thin films. The details of the experimental setup and the data analysis procedure are given in Refs. 64–67. Prior to our thermoreflectance measurements, we metallize our samples with a thin Pt layer as mentioned above. The sample geometry for our thermoreflectance measurements is shown in Fig. 2a. For the analysis, we assume a three-layer thermal model that takes into account the Pt film, the Pt/CTO interface, the CTO film, the CTO/STO interface and the CTO substrate. In doing so, we have lumped the resistances associated with the CSTO confined film (that includes the resistances associated with the CTO/CSTO and CSTO/STO interfaces along with any intrinsic resistance posed by the scattering in the solid-solutions) into a single resistance in the three-layer thermal model. Since there are multiple unknowns in our thermal model, we use a combination of FDTR and TDTR to measure these properties. We note that thermoreflectance techniques used
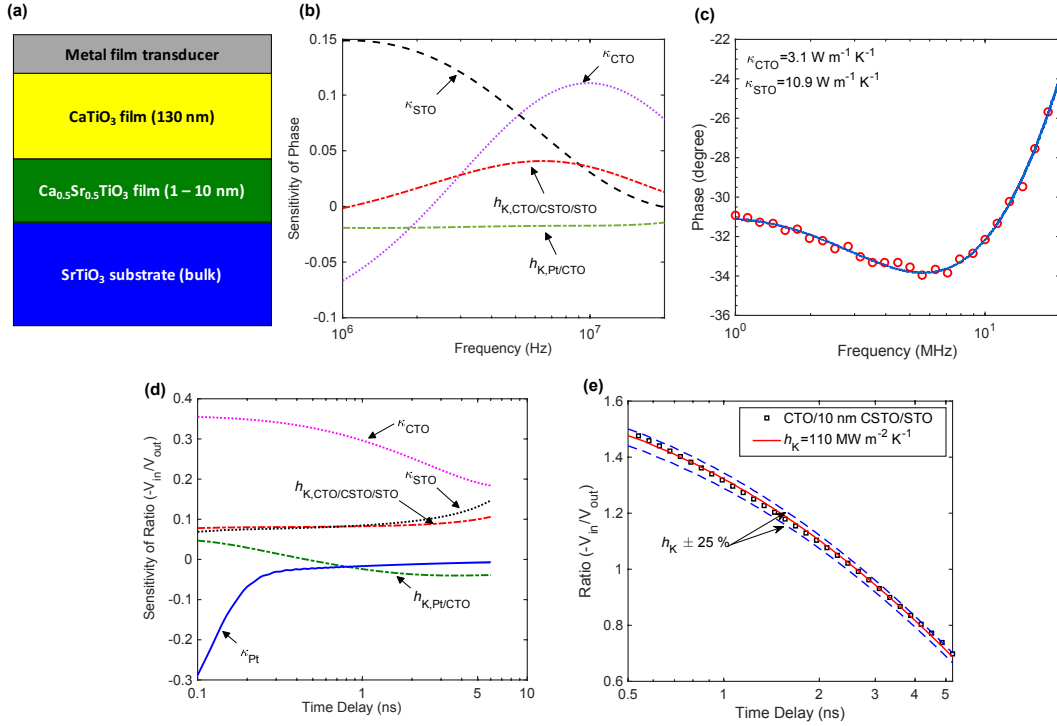
Figure 2: (a) Schematic of our sample geometry (Pt/CaTiO$_3$/Ca$_{0.5}$Sr$_{0.5}$TiO$_3$/SrTiO$_3$) for our thermal measurements via pump-probe time domain thermoreflectance and frequency domain thermoreflectance techniques. (b) Sensitivity of the phase from our FDTR measurements as a function of frequency to the various parameters in our three-layer thermal model. The sensitivity to the thermal conductivities of the CaTiO$_3$ film and SrTiO$_3$ substrates are relatively higher, which allows for their accurate measurements. (c) Characteristic FDTR data shown as a function of pump modulation frequency and analytical model fit to the data for the sample with ~10 nm Ca$_{0.5}$Sr$_{0.5}$TiO$_3$ solid-solution film. (d) Sensitivity of the ratio of in-phase and out-of-phase signals from our TDTR measurements at 7 MHz modulation frequency to the various parameters in our three-layer thermal model. The thermal conductivities of the CaTiO$_3$ film and the STO substrate have relatively higher sensitivities as compared to the thermal boundary conductance at the CaTiO$_3$/Ca$_{0.5}$Sr$_{0.5}$TiO$_3$/SrTiO$_3$ interface. Therefore, these values are accurately determined from the FDTR measurements. (e) Characteristic time domain thermoreflectance data and best-fit curve for the sample with ~10 nm Ca$_{0.5}$Sr$_{0.5}$TiO$_3$ solid-solution film at 7 MHz modulation frequency along with uncertainties (dotted lines).

in this work are mainly sensitive to the cross-plane thermal conductance measurements. Other limitations associated with the techniques have been extensively discussed in Refs. 64,68,69. The most relevant limitation of the techniques pertaining to the current work, however, is the ability to accurately quantify thermal conductances, which will be discussed in more detail below.

Along with the thermal boundary conductance across the solid-solution films, we also measure a room temperature thermal conductivity of 3.1±0.3 W m^{-1} K^{-1} for the ∼130 nm CTO film from the best-fit between the thermal model and our FDTR data. As shown in Fig. 2b, the sensitivities to the thermal conductivities of the CTO film and the STO substrate are much higher as compared to that of the thermal boundary conductance in our FDTR measurements, thus allowing for the accurate measurements of the CTO and STO thermal conductivities; an example of our FDTR fitting routine is shown in Fig. 2b for our confined CSTO solid-solution film with thickness of ∼10 nm. The value of 3.1±0.3 W m^{-1} K^{-1} for the ∼130 nm CTO film is slightly lower than the thermal conductivity of ∼3.9 W m^{-1} K^{-1} for a thicker (200 nm) film from our previous measurements.[70] The reduction in thermal conductivity for the thinner film could be due to size effects and boundary scattering. While an approximation based on the gray-body model predicts a mean-free-path (∼37 nm for CTO calculated based on the heat capacity and sound speed of CTO)[71] that is shorter than the 130 nm CTO film thickness, the mean-free-paths in crystalline materials can span a broad range. For example, a first-principles calculation predicts mean-free-paths in the range of 1 nm - 1 μm for STO.[72] Similar first-principles-based calculations of thermal transport properties for CTO would lend more insight into the mean-free-paths associated with individual phonon modes dictating heat transfer for both bulk and thin films of CTO, which deservers further work but is beyond the scope of the current study. It should be noted that for similar oxide materials, A-site vacancy doping and defects significantly reduce the thermal conductivity and could also be playing a part in our measurement of thermal conductivity of the CTO film;[73–75] a discussion on oxygen vacancies is presented in the Supporting Information. We also measure the room temperature thermal conductivity of 10.9±1.1 W m^{-1} K^{-1} for our STO substrates, which agrees well with previous measurements.[76]

The thermal conductivities of CTO film and STO substrate are used as input parameters in our TDTR measurements used to report the h_K across confined thin films with varying thicknesses. The sensitivities to the thermal conductivities of CTO film and STO substrate in our TDTR measurements (as shown in Fig. 2d at 7 MHz pump modulation frequency) are relatively higher than the sensitivity to h_K at the CTO/CSTO/STO interface, which makes it imperative that we accurately determine these thermal conductivities. Therefore, FDTR measurements, which are mostly sensitive to the thermal conductivities as shown in the sensitivity analysis in Fig. 2b are initially performed to reduce the uncertainty in the measured h_K from our TDTR measurements. Figure 2e shows a representative TDTR measurement for our sample with the 10 nm CSTO solid-solution film along with the best-fit curve of our three-layer thermal model used to back-out h_K across the CTO/CSTO/STO interface. The propagation of uncertainty from the thermal conductivities of CTO film and STO substrate measured via FDTR leads to ~25-30 % uncertainty in the measured h_K as shown by the dashed lines in Fig. 2d. These uncertainties are based on changes in the values of h_K across the CTO/CSTO/STO interfaces as a result of perturbing the different parameters in our three-layer thermal model within their error bounds.

Figure 3a shows our measurements of h_K as a function of the solid-solution film thickness (red squares). For comparison, we also plot h_K measured (via TDTR in Ref. 77) across Al/Cu interfaces where the chemical abruptness of the metal/metal interfaces are systematically varied by ion-beam mixing. We also plot similar measurements on interfaces formed between a metal and a semiconductor (Cr/Si) taken from Ref. 38, where the interface interdiffusion is systematically controlled. Both sets of measurements show a monotonic decrease in h_K as the interfacial layer increases in thickness as a result of intermixing. Even though the electron-driven h_K for the metal/metal interface is significantly higher as compared to the phonon-dominated h_K across the metal/dielectric interface, both studies suggest that diffusive scattering of the energy carriers at the intermixed "alloy region" at the interface lowers h_K as the thickness of the disordered region increases. In contrast, our results for the solid-solution thin films, where thermal transport has no appreciable electronic component, suggest that the addition of interfacial solid-solution films of

11

(a)

Thermal boundary conductance (MW m^{-2} K^{-1})

Al/Cu (Gundrum *et al.*)

Cr/Si (Hopkins *et al.*)

abrupt
interface
CTO/STO

CTO/CSTO/STO

Thickness, *d* (nm)

(b)

Effective thermal conductivity
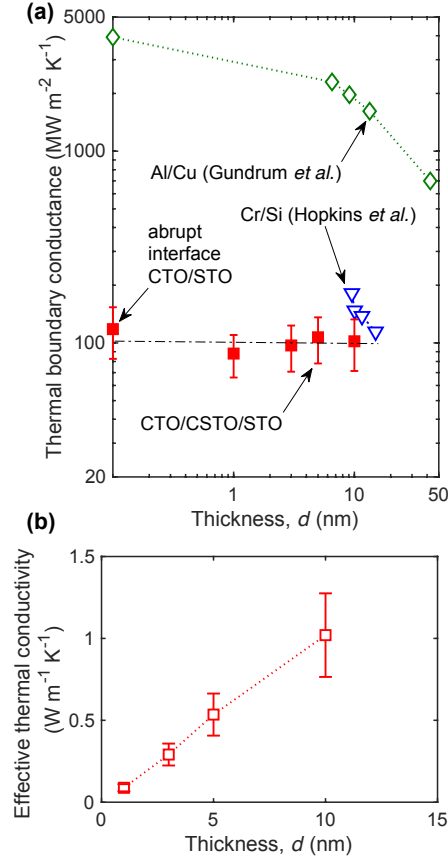(W m^{-1} K^{-1})

Thickness, *d* (nm)

Figure 3: (a) Measured thermal boundary conductance across the confined thin film solid-solutions as a function of thickness of the solid-solutions. For comparison, we also plot the measurements of thermal boundary conductances for Al/Cu and Cr/Si with systematically varying length of the interfacial mixing layer (plotted as the x-axis) from refs. 77 and 38, respectively. Contrary to the prior works, our results for the confined solid-solution films show that adding more material along the heat propagation direction does not lead to lower thermal resistances. (b) Effective thermal conductivities of the confined solid-solution films derived from our thermal boundary conductance measurements.

12

CSTO from $\sim$1 nm to $\sim$10 nm does not lead to a substantial change in h_K.

The relatively similar Debye temperatures between CTO and STO along with approximately 1% lattice constant mismatches between CTO/CSTO and CSTO/STO (suggesting minimal strain at the interface) could partially explain the measured h_K across these interfaces as shown in Fig. 3a; see Supporting Information for discussion on strain and lattice mismatch. However there could be various other competing factors influencing the relatively constant h_K that we measure across the $\sim$1 to 10 nm CSTO thickness. The solid-solution films could provide better overlap in the density of states of energy carrying vibrations between the two materials, which increases h_K at the CTO/CSTO and CSTO/CTO boundaries relative to the CTO/STO interface with minimal intermixing. There could also be an increase in the existence of interfacial modes at the solid-solution film boundaries that can facilitate energy transfer across these interfaces leading to relatively higher conductances across the interfaces of the solid-solution film in comparison to the CTO/STO interfacial conductance as we discuss in more detail below. The other scenario is where phonons with wavelengths longer than the interfacial solid-solution layer transmit across the films and carry most of the heat across the CTO/CSTO/STO interface. In this scenario, the solid-solution films act as if they were transparent, thus resulting in negligible change in h_K with increasing interfacial film thickness. Even though all of these factors could be influencing our measurements, from our results presented in Fig. 3a, we can only assert that diffusive scattering at the disordered interface does not create higher resistance to heat flow as compared to that in an ideal CTO/STO interface. However, to isolate and study the contributions of each of the aforementioned hypotheses in dictating our experimentally measured data, implementation of rigorous computational methods (such as those rooted in molecular dynamics simulations and extensive calculations based on the Landauer formalism) for these material systems could provide the atomic- and mode-level details needed to reveal the microscopic vibrational dynamics and therefore deserves further work. As these types of calculations are beyond the scope of the current experimental work, we attempt to elaborate on the aforementioned hypotheses in the context of the current and previous works that have considered heat transfer across thin interfacial films.

The first of the three reasons presented above has been rigorously studied with various computational methods with the consensus that a better overlap in the heat carrying vibrations from the "vibrational bridge" layer at the interface adds elastic conduction channels that can greatly facilitate heat transfer across the interfacial layers.[32–34,41,42,78] For example, through molecular dynamics (MD) simulations on idealized crystals based on the Lennard-Jones potential, English *et al.* have shown that inserting a thin layer of interfacial film with atomic mass that is in between the range of atomic masses of the confining leads, the thermal resistance at the interfaces can be significantly lowered.[41] They prescribed the enhancement in conductance to a better overlap in the available vibrational frequencies of the leads and the interfacial film, as the phonon frequency is inversely proportional to the atomic mass ($\omega \propto \sqrt{1/m}$). Similarly, through nonequilibrium Green's function calculations, Polanco *et al.* have shown that an intermediate layer between two solids maximizes the conductance through better phonon transmission when its' mass is close to the geometric mean of the two solids.[78] Moreover, thermal conductance across a mass graded interfacial film has been shown to be higher as compared to both an abrupt interface and a 50-50 random alloy interfacial film.[79]

With harmonic *ab initio*-based Green's function calculations, Tian *et al.*[34] showed that the thickness of the intermixing layer at the interface can preferentially increase or decrease the transmission of vibrations depending on the spectral range of frequencies. More specifically, their calculations for an interface between silicon and germanium showed that the transmission of phonons in the spectral range of 6-8 THz is maximized for two-atomic layers of intermixing between the two atomic species, whereas four-atomic layers of intermixing resulted in a higher transmission for frequencies in the ∼3-4 THz range. This difference in the spectral contributions resulted in an overall similar thermal conductances between the two- and four-layer intermixing for the silicon and germanium interfaces.[34] Similar competing effects between the different frequency ranges could be occurring for our solid-solution thin films with different thicknesses, which could potentially explain similarities between the measured h_K for the ∼1 nm to ∼10 nm CSTO solid-solution films.

Our results shown in Fig. 3a suggest that diffusive scattering processes intrinsic to the solid-solution films do not pose as a major resistance to heat flow across these thin films. This is consistent with the picture that mass impurities in solid-solutions lead to scattering of the more dispersive vibrations leaving the effect of long wavelength phonons to have a more pronounced effect in controlling thermal conductivity in solid-solutions. As such, the thermal conductivity of a solid-solution increases as the characteristic length increases. Considering this, we define an effective thermal conductivity for our thin solid-solution films based on our measurements of h_{K} ($\kappa_{\mathrm{eff}}=h_{\mathrm{K}}\cdot d$) and plot the results in Fig. 3b. As is consistent with the above described picture, the effective thermal conductivity of our confined solid-solution films does indeed increase with thickness, thus supporting the argument that resistive processes due to intrinsic scattering of vibrations in the solid-solutions do not impede heat flow across these confined films, and the thermal conductance across the film is mainly ballistic.

As mentioned above, another probable mechanism influencing our results, shown in Fig. 2d, is the emergence of non-propagating interfacial modes. In this context, by performing lattice dynamics and MD simulations, Gordiz *et al.*[30] have shown that along with elastic interactions being the dominant contributors to h_{K} for an interface between amorphous silicon and germanium, interfacial modes can contribute more than 19 % to the total h_{K} across these interfaces. Even though their results could be material specific, and not directly applicable to the perovskite oxide systems considered in this work, the increase in h_{K} across the individual CTO/CSTO and CSTO/STO relative to the CTO/STO interfacial conductance could potentially be driven by an increase in the population of localized interfacial modes at the interfaces with the solid-solution region. Along with interfacial modes, anharmonic scattering at the CTO/CSTO and CSTO/CTO interfaces could also result in a higher conductance relative to the CTO/STO interface. As shown by prior experimental and theoretical works, anharmonic scattering channels can substantially enhance h_{K} across dissimilar materials (at relatively high temperatures where anharmonic processes can dominate thermal transport across materials).[80–83] Such multiple phonon processes abating h_{K} across our CTO/CSTO/STO interfaces with increasing thickness of the solid-solution region could also

have an influence on our measured h_{K}. However, since the Debye temperatures for CTO and STO are relatively much higher than room temperature (the Debye temperatures for un-doped STO and CTO are $\sim$413 K and $\sim$473 K, respectively),[84,85] our measurements of h_{K} across the thin solid-solution films are most probably not affected by these types of higher order anharmonic processes involving multiple phonon scattering processes at the interfacial regions.

We note that further theoretical modeling can lead to insights into phonon transmission and scattering at CTO/CSTO/STO interfaces, which could shed more light into the elastic and inelastic energy interaction channels dictating h_{K} across these interfaces. However, we refrain from applying the often used acoustic and diffuse mismatch models to gain more insight into the mode-level contributions for our experimentally measured h_{K} reported in this work as these approaches have recently been shown to produce erroneous results.[51,80,86] Specifically, these analytical models predict drastically different spectral contributions as compared to predictions from more rigorous models based on MD simulations and first-principles-based calculations.[6] As such, these rigorous computational methods that are able to spectrally decompose the heat flux across interfaces would be needed to potentially reveal the mode-level understanding of phonon transmission and interfacial mode contributions to h_{K} across these oxide perovskite systems, which deserves further work. Moreover, these rigorous computational methods could also reveal the intrinsic phonon mean-free-paths

Conclusions

In summary, we have measured the thermal boundary conductance across single crystalline $CaTiO_3$ (CTO)/$SrTiO_3$ (STO) interfaces with varying thicknesses of single crystalline $Ca_{0.5}Sr_{0.5}TiO_3$ (CSTO) interfacial confined thin solid-solution films. We find that the thicker solid-solutions do not lead to higher overall resistances across the solid-solution interfacial films with the thermal boundary conductances across the CTO/CSTO/STO interfaces relatively constant regardless of the CSTO thickness. Our experimental work reveals direct insight into vibrational energy exchange mechanisms

that dictate energy transfer processes across interfaces. Furthermore, our results could potentially provide validation for prior theoretical works that have shown that a "vibrational bridge" layer can lead to a better overlap in the heat carrying vibrations through additional elastic conduction channels that can greatly facilitate heat transfer across interfacial layers.

Supporting Information

Additional details on sample Root Mean Square (RMS) roughness, lattice mismatch, cation ordering, and oxygen vacancies

References

(1) Einstein, A. Elementare Betrachtungen uber die thermische Molekularbewegung in festen Korpern. *Annalen der Physik* **1911**, *340*, 679.

(2) Cahill, D. G.; Watson, S. K.; Pohl, R. O. Lower Limit to the Thermal Conductivity of Disordered Crystals. *Phys. Rev. B* **1992**, *46*, 6131–6140.

(3) Agne, M. T.; Hanus, R.; Snyder, G. J. Minimum Thermal Conductivity in The Context of Diffuson-Mediated Thermal Transport. *Energy Environ. Sci.* **2018**, *11*, 609–616.

(4) Kapitza, P. L. The Study of Heat Transfer in Helium II. *Zhurnal eksperimentalnoi i teoreticheskoi fiziki* **1941**, *11*, 1–31.

(5) Swartz, E. T.; Pohl, R. O. Thermal Boundary Resistance. *Reviews of Modern Physics* **1989**, *61*, 605–668.

(6) Giri, A.; Hopkins, P. E. A Review of Experimental and Computational Advances in Thermal Boundary Conductance and Nanoscale Thermal Transport across Solid Interfaces. *Advanced Functional Materials* **2019**, *n/a*, 1903857.

(7) Stoner, R. J.; Maris, H. J. Kapitza Conductance and Heat Flow Between Solids at Temperatures From 50 to 300 K. *Phys. Rev. B* **1993**, *48*, 16373–16387.

(8) Stevens, R. J.; Smith, A. N.; Norris, P. M. Measurement of Thermal Boundary Conductance of a Series of Metal-Dielectric Interfaces by the Transient Thermoreflectance Technique. *Journal of Heat Transfer* **2005**, *127*, 315–322.

(9) Lyeo, H.-K.; Cahill, D. G. Thermal Conductance of Interfaces Between Highly Dissimilar Materials. *Phys. Rev. B* **2006**, *73*, 144301.

(10) Costescu, R. M.; Wall, M. A.; Cahill, D. G. Thermal Conductance of Epitaxial Interfaces. *Phys. Rev. B* **2003**, *67*, 054302.

(11) Cheaito, R.; Gaskins, J. T.; Caplan, M. E.; Donovan, B. F.; Foley, B. M.; Giri, A.; Duda, J. C.; Szwejkowski, C. J.; Constantin, C.; Brown-Shaklee, H. J.; Ihlefeld, J. F.; Hopkins, P. E. Thermal Boundary Conductance Accumulation and Interfacial Phonon Transmission: Measurements and Theory. *Phys. Rev. B* **2015**, *91*, 035432.

(12) Duda, J. C.; Hopkins, P. E. Systematically Controlling Kapitza Conductance via Chemical Etching. *Applied Physics Letters* **2012**, *100*, 111602.

(13) Giri, A.; Braun, J. L.; Hopkins, P. E. Implications of Interfacial Bond Strength on the Spectral Contributions to Thermal Boundary Conductance Across Solid, Liquid, and Gas Interfaces: A molecular dynamics study. *The Journal of Physical Chemistry C* **2016**, *120*, 24847–24856.

(14) OBrien, P. J.; Shenogin, S.; Liu, J.; Chow, P. K.; Laurencin, D.; Mutin, P. H.; Yamaguchi, M.; Keblinski, P.; Ramanath, G. Bonding-induced Thermal Conductance Enhancement at Inorganic Heterointerfaces Using Nanomolecular Monolayers. *Nat Mater* **2013**, *12*, 118–122.

(15) Losego, M. D.; Grady, M. E.; Sottos, N. R.; Cahill, D. G.; Braun, P. V. Effects of Chemical Bonding on Heat Transport Across Interfaces. *Nat Mater* **2012**, *11*, 502–506.

(16) Giri, A.; King, S. W.; Lanford, W. A.; Mei, A. B.; Merrill, D.; Li, L.; Oviedo, R.; Richards, J.; Olson, D. H.; Braun, J. L.; Gaskins, J. T.; Deangelis, F.; Henry, A.; Hopkins, P. E. Interfacial Defect Vibrations Enhance Thermal Transport in Amorphous Multilayers with Ultrahigh Thermal Boundary Conductance. *Advanced Materials* **2018**, *30*, 1804097.

(17) Olson, D. H.; Freedy, K. M.; McDonnell, S. J.; Hopkins, P. E. The Influence of Titanium Adhesion Layer Oxygen Stoichiometry on Thermal Boundary Conductance At Gold Contacts. *Applied Physics Letters* **2018**, *112*, 171602.

(18) Freedy, K. M.; Giri, A.; Foley, B. M.; Barone, M. R.; Hopkins, P. E.; McDonnell, S. Titanium Contacts to Graphene: Process-induced Variability in Electronic and Thermal Transport. *Nanotechnology* **2018**, *29*, 145201.

(19) Hsieh, W.-P.; Lyons, A. S.; Pop, E.; Keblinski, P.; Cahill, D. G. Pressure Tuning of the Thermal Conductance of Weak Interfaces. *Phys. Rev. B* **2011**, *84*, 184107.

(20) Monachon, C.; Weber, L.; Dames, C. Thermal Boundary Conductance: A Materials Science Perspective. *Annual Review of Materials Research* **2016**, *46*, 433–463.

(21) Hopkins, P. E.; Beechem, T.; Duda, J. C.; Hattar, K.; Ihlefeld, J. F.; Rodriguez, M. A.; Piekos, E. S. Influence of Anisotropy on Thermal Boundary Conductance at Solid Interfaces. *Phys. Rev. B* **2011**, *84*, 125408.

(22) Giri, A.; Hopkins, P. E. Role of Interfacial Mode Coupling of Optical Phonons on Thermal Boundary Conductance. *Scientific Reports* **2017**, *7*, 11011.

(23) Duda, J. C.; Kimmer, C. J.; Soffa, W. A.; Zhou, X. W.; Jones, R. E.; Hopkins, P. E. Influence of Crystallographic Orientation and Anisotropy on Kapitza Conductance via Classical Molecular Dynamics Simulations. *Journal of Applied Physics* **2012**, *112*, 093515.

(24) Merabia, S.; Termentzidis, K. Thermal Boundary Conductance Across Rough Interfaces Probed by Molecular Dynamics. *Phys. Rev. B* **2014**, *89*, 054309.

(25) Liang, Z.; Sasikumar, K.; Keblinski, P. Thermal Transport across a Substrate–Thin-Film Interface: Effects of Film Thickness and Surface Roughness. *Phys. Rev. Lett.* **2014**, *113*, 065901.

(26) Jeong, M.; Freedman, J. P.; Liang, H. J.; Chow, C.-M.; Sokalski, V. M.; Bain, J. A.; Malen, J. A. Enhancement of Thermal Conductance at Metal-Dielectric Interfaces using Sub-nanometer Metal Adhesion Layers. *Phys. Rev. Applied* **2016**, *5*, 014009.

(27) Saha, D.; Yu, X.; Jeong, M.; Darwish, M.; Weldon, J.; Gellman, A. J.; Malen, J. A. Impact of Metal Adhesion Layer Diffusion on Thermal Interface Conductance. *Phys. Rev. B* **2019**, *99*, 115418.

(28) Xu, Y.; Kato, R.; Goto, M. Effect of Microstructure on Au/sapphire Interfacial Thermal Resistance. *Journal of Applied Physics* **2010**, *108*, 104317.

(29) Giri, A.; Donovan, B. F.; Hopkins, P. E. Localization of Vibrational Modes Leads to Reduced Thermal Conductivity of Amorphous Heterostructures. *Phys. Rev. Materials* **2018**, *2*, 056002.

(30) Gordiz, K.; Henry, A. Phonon Transport at Interfaces between Different Phases of Silicon and Germanium. *Journal of Applied Physics* **2017**, *121*, 025102.

(31) Li, R.; Gordiz, K.; Henry, A.; Hopkins, P. E.; Lee, E.; Luo, T. Effect of Light Atoms on Thermal Transport across Solid–Solid Interfaces. *Phys. Chem. Chem. Phys.* **2019**, *21*, 17029–17035.

(32) Duda, J. C.; English, T. S.; Piekos, E. S.; Beechem, T. E.; Kenny, T. W.; Hopkins, P. E. Bidirectionally Tuning Kapitza Conductance through the Inclusion of Substitutional Impurities. *Journal of Applied Physics* **2012**, *112*, 073519.

(33) Stevens, R. J.; Zhigilei, L. V.; Norris, P. M. Effects of Temperature and Disorder on Thermal Boundary Conductance at Solid–Solid Interfaces: Nonequilibrium molecular dynamics simulations. *International Journal of Heat and Mass Transfer* **2007**, *50*, 3977 – 3989.

(34) Tian, Z.; Esfarjani, K.; Chen, G. Enhancing Phonon Transmission Across a Si/Ge Interface by Atomic Roughness: First-principles Study with the Green's Function Method. *Phys. Rev. B* **2012**, *86*, 235304.

(35) Hopkins, P. E. Thermal Transport across Solid Interfaces with Nanoscale Imperfections: Effects of Roughness, Disorder, Dislocations, and Bonding on Thermal Boundary Conductance. *ISRN Mechanical Engineering* **2013**, 682586.

(36) Duda, J. C.; Yang, C.-Y. P.; Foley, B. M.; Cheaito, R.; Medlin, D. L.; Jones, R. E.; Hopkins, P. E. Influence of Interfacial Properties on Thermal Transport at Gold:Silicon Contacts. *Applied Physics Letters* **2013**, *102*, 081902.

(37) Hopkins, P. E.; Phinney, L. M.; Serrano, J. R.; Beechem, T. E. Effects of Surface Roughness and Oxide Layer on the Thermal Boundary Conductance at Aluminum/Silicon Interfaces. *Phys. Rev. B* **2010**, *82*, 085307.

(38) Hopkins, P. E.; Norris, P. M.; Stevens, R. J.; Beechem, T. E.; Graham, S. Influence of Interfacial Mixing on Thermal Boundary Conductance across a Chromium/Silicon Interface. *Journal of Heat Transfer* **2008**, *130*, 062402–062402.

(39) Yeandel, S. R.; Molinari, M.; Parker, S. C. Nanostructuring Perovskite Oxides: the Impact of SrTiO$_3$ nanocube 3D Self-Assembly on Thermal Conductivity. *RSC Adv.* **2016**, *6*, 114069–114077.

(40) Yeandel, S. R.; Molinari, M.; Parker, S. C. The impact of Tilt Grain Boundaries on the Thermal Transport in Perovskite SrTiO$_3$ Layered Nanostructures. A Computational Study. *Nanoscale* **2018**, *10*, 15010–15022.

(41) English, T. S.; Duda, J. C.; Smoyer, J. L.; Jordan, D. A.; Norris, P. M.; Zhigilei, L. V. Enhancing and Tuning Phonon Transport at Vibrationally Mismatched Solid-Solid Interfaces. *Phys. Rev. B* **2012**, *85*, 035438.

(42) Rastgarkafshgarkolaei, R.; Zhang, J.; Polanco, C. A.; Le, N. Q.; Ghosh, A. W.; Norris, P. M. Maximization of Thermal Conductance at Interfaces via Exponentially Mass-Graded Interlayers. *Nanoscale* **2019**, *11*, 6254–6262.

(43) Gorham, C. S.; Hattar, K.; Cheaito, R.; Duda, J. C.; Gaskins, J. T.; Beechem, T. E.; Ihlefeld, J. F.; Biedermann, L. B.; Piekos, E. S.; Medlin, D. L.; Hopkins, P. E. Ion Irradiation of the Native Oxide/Silicon Surface Increases the Thermal Boundary Conductance across Aluminum/Silicon interfaces. *Phys. Rev. B* **2014**, *90*, 024301.

(44) Giri, A.; Hopkins, P. E.; Wessel, J. G.; Duda, J. C. Kapitza Resistance and the Thermal Conductivity of Amorphous Superlattices. *Journal of Applied Physics* **2015**, *118*, 165303.

(45) Giri, A.; Braun, J. L.; Hopkins, P. E. Effect of Crystalline/Amorphous Interfaces on Thermal Transport across Confined Thin Films and Superlattices. *Journal of Applied Physics* **2016**, *119*.

(46) Kimling, J.; Philippi-Kobs, A.; Jacobsohn, J.; Oepen, H. P.; Cahill, D. G. Thermal Conductance of Interfaces with Amorphous SiO_2 Measured by Time-Resolved Magneto-Optic Kerr-Effect Thermometry. *Phys. Rev. B* **2017**, *95*, 184305.

(47) Fong, S. W.; Sood, A.; Chen, L.; Kumari, N.; Asheghi, M.; Goodson, K. E.; Gibson, G. A.; Wong, H.-S. P. Thermal Conductivity Measurement of Amorphous Dielectric Multilayers for Phase-Change Memory Power Reduction. *Journal of Applied Physics* **2016**, *120*, 015103.

(48) Beechem, T.; Hopkins, P. E. Predictions of Thermal Boundary Conductance for Systems of Disordered Solids and Interfaces. *Journal of Applied Physics* **2009**, *106*.

(49) Gordiz, K.; Henry, A. Phonon Transport at Crystalline Si/Ge Interfaces: The Role of Interfacial Modes of Vibration. *Scientific Reports* **2016**, *6*, 23139.

(50) Gordiz, K.; Henry, A. Phonon transport at interfaces: Determining the correct modes of vibration. *Journal of Applied Physics* **2016**, *119*.

(51) Feng, T.; Zhong, Y.; Shi, J.; Ruan, X. Unexpected High Inelastic Phonon Transport across Solid-Solid Interface: Modal Nonequilibrium Molecular Dynamics Simulations and Landauer Analysis. *Phys. Rev. B* **2019**, *99*, 045301.

(52) Aller, H. T.; Yu, X.; Wise, A.; Howell, R. S.; Gellman, A. J.; McGaughey, A. J. H.; Malen, J. A. Chemical Reactions Impede Thermal Transport Across Metal Ga2O3 Interfaces. *Nano Letters* **2019**, *19*, 8533–8538.

(53) Wang, R. Y.; Segalman, R. A.; Majumdar, A. Room Temperature Thermal Conductance of Alkanedithiol Self-Assembled Monolayers. *Applied Physics Letters* **2006**, *89*, 173113.

(54) Duda, J. C.; Saltonstall, C. B.; Norris, P. M.; Hopkins, P. E. Assessment and Prediction of Thermal Transport at Solid-self-assembled Monolayer Junctions. *The Journal of Chemical Physics* **2011**, *134*, –.

(55) Majumdar, S.; Sierra-Suarez, J. A.; Schiffres, S. N.; Ong, W.-L.; C. Fred Higgs, I.; McGaughey, A. J. H.; Malen, J. A. Vibrational Mismatch of Metal Leads Controls Thermal Conductance of Self-assembled Monolayer Junctions. *Nano Letters* **2015**, *15*, 2985–2991.

(56) Cheaito, R.; Duda, J. C.; Beechem, T. E.; Hattar, K.; Ihlefeld, J. F.; Medlin, D. L.; Rodriguez, M. A.; Campion, M. J.; Piekos, E. S.; Hopkins, P. E. Experimental Investigation of Size Effects on the Thermal Conductivity of Silicon-Germanium Alloy Thin Films. *Phys. Rev. Lett.* **2012**, *109*, 195901.

(57) Mannhart, J.; Schlom, D. G. Oxide Interfaces—An Opportunity for Electronics. *Science* **2010**, *327*, 1607–1611.

(58) Reyren, N.; Thiel, S.; Caviglia, A. D.; Kourkoutis, L. F.; Hammerl, G.; Richter, C.; Schneider, C. W.; Kopp, T.; Rüetschi, A.-S.; Jaccard, D.; Gabay, M.; Muller, D. A.; Triscone, J.-M.; Mannhart, J. Superconducting Interfaces Between Insulating Oxides. *Science* **2007**, *317*, 1196–1199.

(59) Brinkman, A.; Huijben, M.; van Zalk, M.; Huijben, J.; Zeitler, U.; Maan, J. C.; van der Wiel, W. G.; Rijnders, G.; Blank, D. H. A.; Hilgenkamp, H. Magnetic Effects at the Interface between Non-magnetic Oxides. *Nature Materials* **2007**, *6*, 493–496.

(60) Ohtomo, A.; Hwang, H. Y. A High-mobility Electron Gas at the $LaAlO_3$/$SrTiO_3$ Heterointerface. *Nature* **2004**, *427*, 423–426.

(61) Wu, S.; Luo, X.; Turner, S.; Peng, H.; Lin, W.; Ding, J.; David, A.; Wang, B.; Van Tendeloo, G.; Wang, J.; Wu, T. Nonvolatile Resistive Switching in Pt/$LaAlO_3$/$SrTiO_3$ Heterostructures. *Phys. Rev. X* **2013**, *3*, 041027.

(62) Lin, W.-N.; Ding, J.-F.; Wu, S.-X.; Li, Y.-F.; Lourembam, J.; Shannigrahi, S.; Wang, S.-J.; Wu, T. Electrostatic Modulation of $LaAlO_3$/$SrTiO_3$ Interface Transport in an Electric Double-Layer Transistor. *Advanced Materials Interfaces* **2014**, *1*, 1300001.

(63) Koster, G.; Kropman, B. L.; Rijnders, G. J. H. M.; Blank, D. H. A.; Rogalla, H. Quasi-ideal Strontium Titanate Crystal Surfaces through Formation of Strontium Hydroxide. *Applied Physics Letters* **1998**, *73*, 2920–2922.

(64) Hopkins, P. E.; Serrano, J. R.; Phinney, L. M.; Kearney, S. P.; Grasser, T. W.; Harris, C. T. Criteria for Cross-plane Dominated Thermal Transport in Multilayer Thin Film Systems during Modulated Laser Heating. *J. Heat Transfer* **2010**, *132*, 081302.

(65) Schmidt, A.; Chiesa, M.; Chen, X.; Chen, G. An Optical Pump-probe Technique for Measuring the Thermal Conductivity of Liquids. *Rev. Sci. Instrum.* **2008**, *79*, 064902.

(66) Cahill, D. G. Analysis of Heat Flow in Layered Structures for Time-domain Thermoreflectance Analysis of Heat flow in Layered Structures for Time-domain Thermoreflectance. *Rev. Sci. Instrum.* **2004**, *75*, 5119–5122.

(67) Cheaito, R. The Role of Siize Effects on the Thermal Conductivity of Thin Film Alloys

and Superlattices. Ph.D. thesis, School of Engineering and Applied Science, University of Virginia, 2015.

(68) Jiang, P.; Qian, X.; Yang, R. Tutorial: Time-Domain Thermoreflectance (TDTR) for Thermal Property Characterization of Bulk and Thin Film Materials. *Journal of Applied Physics* **2018**, *124*, 161103.

(69) Olson, D. H.; Braun, J. L.; Hopkins, P. E. Spatially Resolved Thermoreflectance Techniques for Thermal Conductivity Measurements from the Nanoscale to the Mesoscale. *Journal of Applied Physics* **2019**, *126*, 150901.

(70) Ravichandran, J.; Yadav, A. J.; Cheaito, R.; Rossen, P. B.; Soukiassian, A.; Suresha, S., J.; Duda, J. C.; Foley, B. M.; Lee, C.-H.; Zhu, Y.; Lichtenberger, A. W.; Moore, J. E.; Muller, D. A.; Schlom, D. G.; Hopkins, P. E; Majumdar, A.; Ramamoorthy, R.; Zurbuchen; M. A. Crossover from Incoherent to Coherent Phonon Scattering in Epitaxial Oxide Superlattices. *Nat Mater* **2014**, *13*, 168–172.

(71) Gillet, P.; Guyot, F.; Price, G. D.; Tournerie, B.; Le Cleach, A. Phase Changes and Thermodynamic Properties of $CaTiO_3$. Spectroscopic Data, Vibrational Modelling and some Insights on the Properties of $MgSiO_3$ Perovskite. *Physics and Chemistry of Minerals* **1993**, *20*, 159–170.

(72) Feng, L.; Shiga, T.; Shiomi, J. Phonon Transport in Perovskite $SrTiO_3$ from First Principles. *Applied Physics Express* **2015**, *8*, 071501.

(73) Azough, F.; Cernik, R. J.; Schaffer, B.; Kepaptsoglou, D.; Ramasse, Q. M.; Bigatti, M.; Ali, A.; MacLaren, I.; Barthel, J.; Molinari, M.; Baran, J. D.; Parker, S. C.; Freer, R. Tungsten Bronze Barium Neodymium Titanate ($Ba_{6-3n}Nd_{8+2n}Ti_{18}O_{54}$): An Intrinsic Nanostructured Material and Its Defect Distribution. *Inorganic Chemistry* **2016**, *55*, 3338–3350.

(74) Azough, F.; Freer, R.; Yeandel, S. R.; Baran, J. D.; Molinari, M.; Parker, S. C.; Guilmeau, E.; Kepaptsoglou, D.; Ramasse, Q.; Knox, A.; Gregory, D.; Paul, D.; Paul, M.; Montecucco, A.;

Siviter, J.; Mullen, P.; Li, W.; Han, G.; Man, E. A.; Baig, H.; Mallick, T.; Sellami, N.; Min, G.; Sweet, T. Tungsten Bronze: A New High-Temperature n-Type Oxide Thermoelectric. *Journal of Electronic Materials* **2016**, *45*, 1894–1899.

(75) Azough, F.; Jackson, S. S.; Ekren, D.; Freer, R.; Molinari, M.; Yeandel, S. R.; Panchmatia, P. M.; Parker, S. C.; Maldonado, D. H.; Kepaptsoglou, D. M.; Ramasse, Q. M. Concurrent La and A-Site Vacancy Doping Modulates the Thermoelectric Response of SrTiO3: Experimental and Computational Evidence. *ACS Applied Materials & Interfaces* **2017**, *9*, 41988–42000.

(76) Yu, C.; Scullin, M. L.; Huijben, M.; Ramesh, R.; Majumdar, A. Thermal Conductivity Reduction in Oxygen-deficient Strontium Titanates. *Applied Physics Letters* **2008**, *92*, 191911.

(77) Gundrum, B. C.; Cahill, D. G.; Averback, R. S. Thermal Conductance of Metal-metal Interfaces. *Phys. Rev. B* **2005**, *72*, 245426.

(78) Polanco, C. A.; Rastgarkafshgarkolaei, R.; Zhang, J.; Le, N. Q.; Norris, P. M.; Ghosh, A. W. Design Rules for Interfacial Thermal Conductance: Building Better Bridges. *Phys. Rev. B* **2017**, *95*, 195303.

(79) Zhou, Y.; Zhang, X.; Hu, M. An Excellent Candidate for Largely Reducing Interfacial Thermal Resistance: A Nano-confined Mass Graded Interface. *Nanoscale* **2016**, *8*, 1994–2002.

(80) Gaskins, J. T.; Kotsonis, G.; Giri, A.; Ju, S.; Rohskopf, A.; Wang, Y.; Bai, T.; Sachet, E.; Shelton, C. T.; Liu, Z.; Cheng, Z.; Foley, B. M.; Graham, S.; Luo, T.; Henry, A.; Goorsky, M. S.; Shiomi, J.; Maria, J.-P.; Hopkins, P. E. Thermal Boundary Conductance Across Heteroepitaxial ZnO/GaN Interfaces: Assessment of the Phonon Gas Model. *Nano Letters* **2018**, *18*, 7469–7477.

(81) Hohensee, G. T.; Wilson, R. B.; Cahill, D. G. Thermal Conductance of Metal–Diamond Interfaces at High Pressure. *Nat Commun* **2015**, *6*.

(82) Hopkins, P. E. Multiple Phonon Processes Contributing to Inelastic Scattering during Thermal Boundary Conductance at Solid Interfaces. *Journal of Applied Physics* **2009**, *106*, 013528.

(83) Hopkins, P. E.; Duda, J. C.; Norris, P. M. Anharmonic Phonon Interactions at Interfaces and Contributions to Thermal Boundary Conductance. *Journal of Heat Transfer* **2011**, *133*, 062401.

(84) Lawless, W. N. Debye Temperatures of Ferroelectrics. *Phys. Rev. B* **1978**, *17*, 1458–1459.

(85) Knight, K. S. Structural and Thermoelastic Properties of $CaTiO_3$ Perovskite between 7K and 400K. *Journal of Alloys and Compounds* **2011**, *509*, 6337–6345.

(86) Hua, C.; Chen, X.; Ravichandran, N. K.; Minnich, A. J. Experimental Metrology to Obtain Thermal Phonon Transmission Coefficients at Solid Interfaces. *Phys. Rev. B* **2017**, *95*, 205423.

Acknowledgement

Graphical TOC Entry